AIP | The Journal of Chemical Physics

A new approach to calculate charge carrier transport mobility in organic molecular crystals from imaginary time path integral simulations

Linze Song and Qiang Shi

Citation: The Journal of Chemical Physics **142**, 174103 (2015); doi: 10.1063/1.4919061
View online: http://dx.doi.org/10.1063/1.4919061
View Table of Contents: http://scitation.aip.org/content/aip/journal/jcp/142/17?ver=pdfcov
Published by the AIP Publishing

A new approach to calculate charge carrier transport mobility in organic molecular crystals from imaginary time path integral simulations

Linze Song and Qiang Shi[a)]
Beijing National Laboratory for Molecular Sciences, State Key Laboratory for Structural Chemistry of Unstable and Stable Species, Institute of Chemistry, Chinese Academy of Sciences, Zhongguancun, Beijing 100190, China

(Received 16 January 2015; accepted 15 April 2015; published online 4 May 2015)

We present a new non-perturbative method to calculate the charge carrier mobility using the imaginary time path integral approach, which is based on the Kubo formula for the conductivity, and a saddle point approximation to perform the analytic continuation. The new method is first tested using a benchmark calculation from the numerical exact hierarchical equations of motion method. Imaginary time path integral Monte Carlo simulations are then performed to explore the temperature dependence of charge carrier delocalization and mobility in organic molecular crystals (OMCs) within the Holstein and Holstein-Peierls models. The effects of nonlocal electron-phonon interaction on mobility in different charge transport regimes are also investigated. © *2015 AIP Publishing LLC*. [http://dx.doi.org/10.1063/1.4919061]

I. INTRODUCTION

As a novel type of functional materials with promise, organic semiconductors have attracted a lot of research interests over the past decades, with successful applications including organic light emitting diodes (OLEDs),[1] organic field effect transistors(OFETs),[2–4] and organic photovoltaic cells.[5,6] In many aspects, their successful applications depend critically on good charge carrier transport properties.[3,7] As highly ordered structure is favorable in investigating the structure-function relations, single organic molecular crystals (OMCs) tend to be ideal materials for understanding how the charge carriers move in organic materials.[8] However, since Holstein's seminal paper,[9] the mechanism of charge carrier transport in OMCs still challenges theoretical physicists and chemists, despite the many theoretical progress.[10–13]

In comparison to the inorganic semiconductors, molecules in the OMCs are held together by the weak van der Waals interactions. The electron-phonon interactions also play a significant role in determining the charge carrier mobility in OMCs.[10,11,14–17] It is generally believed that the band theory is no longer appropriate to describe the charge carrier motion in OMCs. However, in some experiments, the mobility decreases monotonously with a power-law as the temperature increases, showing a band-like behavior.[3,18] Yet the band theory becomes invalid at relative high temperature because it predicts a mean free path similar to the size of a unit cell.[19] Although we note that the theory based on tunneling enabled hopping can explain the band-like temperature dependence in certain parameter regimes,[20] a unified theory to resolve the above problems is still needed.

The electron-phonon couplings in OMCs are usually classified into two different types. The local electron-phonon coupling causes site energy fluctuations and can be modeled with the Holstein model.[9,14] The nonlocal electron-phonon coupling causes fluctuations of the transfer integrals, and the combined effect of local and nonlocal electron-phonon couplings can be described with the Holstein-Peierls model.[21,22] Munn and Silbey[22,23] have investigated contributions of different types of electron-phonon couplings on the charge carrier mobility based on polaron transformation and a subsequent perturbative calculation of the scattering and hopping contributions to the diffusion constant. They found that the nonlocal electron-phonon couplings often increase the hopping contribution while decrease the band contribution to the mobility. Hannewald *et al.*[21,24,25] have derived a charge carrier mobility expression of Holstein-Peierls model based on the Kubo formula using a polaron transformation similar to Munn and Silbey. They have also evaluated the charge carrier mobility of naphthalene single crystal using parameters from first-principle calculations.[21,26] However, this method also employs perturbation treatment of the polaron transformed Hamiltonian.

Besides the above analytical theories, numerical simulations of the charge carrier mobilities have also been performed. Many of such works are based on mean-field type treatment of the electron-phonon interaction. For example, Troisi and Orlandi[27] considered a model with only nonlocal electron-phonon couplings. Their results show that the scattering caused by fluctuations of the transfer integral leads to band-like transport where charge carrier mobility decreases as the temperature increases. Hultell and Stafström[28] have also investigated the charge carrier motion in the presence of an external electric field using a similar method but with only local electron-phonon couplings. However, it is found recently that the mean field approximation may have some problems in the hopping regime, by comparing to the polaron transformation approach and surface hopping simulations.[29,30]

According to the Kubo formula for the charge carrier mobility, the mobility can be obtained by the time integral of

a)qshi@iccas.ac.cn

the current-current correlation function.[31] From the computational point of view, the difficulty to calculate the (real time) current-current correlation function lies in solving the time dependent quantum dynamics of the multidimensional system, which is still a challenging problem in theoretical chemistry, despite the considerable progress made to simulate real-time quantum dynamics in condensed phase.[32] On the other hand, the equilibrium properties are much easier to calculate using the imaginary time path integral method.[33] In the literature, a widely used method is to perform numerical analytic continuation of the imaginary time correlation function to obtain the real time one.[34–37] However, many numerical analytical continuation methods are often unstable, making it difficult to find a general method that works for different kinds of problems.

In calculation of the charge carrier mobility, only the time integral of the real time correlation function is needed, and the main contribution of the integral comes from the saddle point.[38] So we can apply the saddle point approximation (SPA) to get the time integral based on the imaginary time correlation function, as has been employed by Wolynes in calculating the electron transfer rate.[39] Similar ideas have also been proposed to obtain quantum reaction rate using zero time value and derivatives of the correlation functions from imaginary time path integral calculations.[40–42] Recently, the idea of SPA has been applied in several problems. For example, Yang and Cao have extended the SPA to include higher order time derivatives and apply it to calculations of the electron transfer rate.[43] We have also used the SPA method to calculate hopping rates between neighbouring molecules in OMCs and compared with Fermi's golden rule (FGR) method based on second order perturbation.[44]

In this work, we extend the analytical continuation method to calculate the charge carrier mobility in OMCs, within both the Holstein and Holstein-Peierls models. As in previous works,[39,43] we first shift the integral path to the saddle point on the imaginary time axis and perform path integral Monte Carlo (PIMC) calculations based on the method by Cao *et al.*[45] to obtain the imaginary time correlation function. The SPA is then applied to get the approximate real time correlation function. For the Holstein model with only local electron-phonon couplings, the resulted approximate correlation function is of a Gaussian form as in previous calculation of the electron transfer rate.[39] For the case of Holstein-Peierls model with both local and nonlocal electron-phonon couplings, we have used a new ansatz to perform the analytical continuation. To test the validity of the analytical continuation method, we have also compared the results from the current work with numerical exact calculations using the hierarchical equations of motion (HEOMs) method for the Holstein model.

The remaining sections of this paper are arranged as follows. The total Hamiltonian of the Holstein and Holstein-Peierls models, the imaginary time path integral method used in this work, and the new analytical continuation method to calculate the current-current correlation functions are presented in Sec. II. In Sec. III, we first test the validity of the analytical continuation method using benchmark calculations using the HEOM method and compare the results with the mobility expression from second order perturbation theory, which, in the case of the Holstein model, is identical to the mobility expression by Hannewald and Bobbert.[21,24] Calculations of charge carrier mobilities in different parameter regimes are then presented, where the temperature dependence of charge carrier delocalization and mobility, as well as the effect of non-local electron-phonon coupling on charge carrier transport is investigated. Conclusions and discussions are made in Sec. IV.

II. THEORY

A. Model Hamiltonian

To investigate charge carrier transport properties in OMCs, we employ the Holstein Hamiltonian and its extension that includes the nonlocal electron-phonon couplings (Peierls terms) in a one-dimensional tight-binding model. The total Hamiltonian consists of three terms describing the electronic degrees of freedom (DOFs), the phonon DOFs, and the couplings between them,

$$H = H_e + H_{ph} + H_{e-ph}. \tag{1}$$

The electronic Hamiltonian H_e can be written as

$$H_e = \sum_{m=1}^{N} \varepsilon_m |m\rangle\langle m| - J \sum_{m=1}^{N} (|m\rangle\langle m+1| + |m+1\rangle\langle m|), \tag{2}$$

where $|m\rangle$ denotes a state where the charge carrier is located at the mth site. ε_m is the site energy which is supposed to be the same for all sites and is subsequently set to zero throughout this paper and J denotes the coupling between neighboring sites. We also employ the periodic boundary condition, such that $|N+m\rangle = |m\rangle$.

H_{ph} describes the phonon Hamiltonian. Here, we assume that the charged state at different sites couples with the phonon bath independently, such that H_{ph} can be written as

$$H_{ph} = \sum_{m=1}^{N} \sum_{j=1}^{N_b^m} \left(\frac{p_{mj}^2}{2M_m} + \frac{1}{2} M_m \omega_{mj}^2 x_{mj}^2 \right), \tag{3}$$

where p_{mj}, x_{mj}, M_m, and ω_{mj} are the momentum, displacement, mass, and frequency of the jth harmonic oscillator mode at site m. N_b^m is the number of the bath mode at the site m.

The H_{e-ph} term describes the interaction between the electron and phonon DOFs, which plays an important role in charge carrier dynamics in OMCs. Two different types of interactions are considered. The Holstein model includes the local electron-phonon coupling that causes fluctuations of the site energies, which can be described as

$$H_{e-ph}^{local} = \sum_{m=1}^{N} \sum_{j}^{N_b^m} \alpha_{mj}^{(1)} x_{mj} |m\rangle\langle m|. \tag{4}$$

For the nonlocal electron-phonon interactions, the transfer integrals are modulated by vibrational motion. Such terms can be incorporated in the Peierls Hamiltonian,[22]

$$H_{e-ph}^{nonlocal} = \sum_{m=1}^{N} \sum_{j}^{N_b^m} \alpha_{mj}^{(2)} x_{mj} (|m\rangle\langle m+1| + |m+1\rangle\langle m|). \tag{5}$$

In this work, we assume that the local and nonlocal electron-phonon interactions are not correlated, i.e., for a specific vibrational coordinate x_{mj}, either $\alpha^{(1)}_{mj}$ or $\alpha^{(2)}_{mj}$ is zero. The form of nonlocal electron-phonon couplings in Eq. (5) is also slightly different from those used in previous works.[27,29,30] We note that generalization of the current work to such models is straightforward.

B. Charge carrier mobility

In OMCs, due to the relatively weak electronic coupling and strong electron-phonon interactions, the intrinsic charge carriers is not bare electrons or holes, but the combination of electrons/holes and the lattice distortions around them, i.e., polarons. There are different methods to calculate the charge carrier mobilities in OMCs. A popular method is to calculate the diffusion constant of the charge carrier and then obtain the mobility though the Einstein relationship.[7]

In this work, we use Kubo's expression to directly calculate the dc-mobility based on the linear response theory, in which the mobility is calculated as[31]

$$\mu = \frac{1}{2k_BTe_0}\lim_{\omega\to 0}\int_{-\infty}^{+\infty} dt e^{i\omega t}\langle \tilde{j}(t)\tilde{j}(0)\rangle, \tag{6}$$

where k_B is Boltzmann constant and the current operator $\tilde{j} = \frac{dP}{dt} = \frac{1}{i\hbar}[P,H]$ with the polarization operator P defined as $P = e_0\sum_m R_m|m\rangle\langle m|$.

By defining $R = R_{m+1} - R_m$, where the R_m denotes the coordinate of the mth site, $\tilde{j} = \frac{e_0R}{\hbar}j$, and using the Holstein-Peierls model Hamiltonian in Eqs. (2)–(5), we can get

$$j = -i\sum_m E_m(|m\rangle\langle m+1| - |m+1\rangle\langle m|), \tag{7}$$

where $E_m = -J + \sum_j \alpha^{(2)}_{mj}x_{mj}$. The charge carrier mobility can then be calculated as

$$\begin{aligned}\mu &= \frac{e_0R^2}{2k_BT\hbar^2}\int_{-\infty}^{+\infty} dt\,\langle j(t)j(0)\rangle \\ &= \frac{e_0R^2}{2k_BT\hbar^2}\int_{-\infty}^{+\infty} dt C(t) = \frac{e_0R^2}{2k_BT\hbar^2}K.\end{aligned} \tag{8}$$

The key quantity in the above equations for the charge carrier mobility is the current-current correlation function $C(t) = \langle j(t)j(0)\rangle$. A direct calculation of $C(t)$ in OMCs is still a challenging task. In the literature, Hannewald *et al.* have applied the perturbation theory based on the polaron transformed Hamiltonian.[25] In this work, we employ the analytical continuation method to calculate the current-current correlation function by performing the SPA. As in the previous work by Wolynes,[39] we assume that $C(t)$ is defined on the complex time plane and shifts the integral path of K to the saddle point τ_{st} on the imaginary time axis,

$$K = \int_{\tau_{st}-\infty}^{\tau_{st}+\infty} C(\tau_{st}+t)dt, \tag{9}$$

where t is a real variable.

In the problems considered in this work, it can be shown that the saddle point locates at $\tau_{st} = -\frac{i\hbar\beta}{2}$.[39] We thus note that the shift of integral path in Eq. (9) is equivalent to calculate the symmetrized current-current correlation function, $C(\tau_{st}+t) = C^{sym}(t)$,[46,47] where

$$C^{sym}(t) = \mathrm{Tr}[j(t)e^{-\beta H/2}j(0)e^{-\beta H/2}]. \tag{10}$$

In Eq. (6), the mobility is calculated using the zero frequency value of the Fourier transform of the correlation function $C(t)$, so change of the integral path does not change the value of μ. We then apply the SPA for the Holstein model, by first assuming $C(t) = e^{i\phi(t)}$, then we have

$$K \approx \int_{\tau_{st}-\infty}^{\tau_{st}+\infty} e^{i\phi(\tau_{st})+i\frac{1}{2}\phi''(\tau_{st})t^2} = \sqrt{\frac{2\pi}{-i\phi''(\tau_{st})}}e^{i\phi(\tau_{st})}, \tag{11}$$

where $e^{i\phi(\tau_{st})} = C(\tau_{st})$ and $\phi''(\tau_{st})$ can be calculated from the relation (using the fact that $\phi'(\tau_{st}) = 0$)

$$C''(\tau_{st}) = ie^{i\phi(\tau_{st})}\phi''(\tau_{st}). \tag{12}$$

We note that the second order derivatives of ϕ and C are taken over the real time t on the shifted integral path.

If we define the imaginary time correlation function $G(\tau)$ as

$$\begin{aligned}G(\tau) &\equiv C(-i\tau) = \langle j(-i\tau)j(0)\rangle \\ &= \frac{1}{Z}\mathrm{Tr}(e^{-\beta H}e^{\tau H}j(0)e^{-\tau H}j(0)),\end{aligned} \tag{13}$$

we have $C(\tau_{st}) = G(i\tau_{st})$ and $C''(\tau_{st}) = -G''(i\tau_{st})$, where $i\tau_{st}$ is real, and the second order derivative in G is taken along the imaginary time axis.

We then have the following expression of mobility within the SPA:

$$\mu = \frac{e_0R^2}{2k_BT\hbar^2}G(i\tau_{st})\sqrt{\frac{2\pi}{G''(i\tau_{st})/G(i\tau_{st})}}. \tag{14}$$

We note that the above approximation in Eq. (11) to obtain Eq. (14) is equivalent to a Gaussian approximation for the symmetrized real-time correlation function in Eq. (10). In order to calculate the charge carrier mobility in the Holstein-Peierls model, the following ansatz for the symmetrized correlation function is used:

$$C(\tau_{st}+t) = (c+at^2)e^{bt^2}. \tag{15}$$

This form of ansatz can be justified by analyzing the short time expansion of the perturbation theory (FGR) presented in Appendix A.

The charge carrier mobility for the Holstein-Peierls model can then be calculated from Eqs. (6) and (15) as

$$\mu = \frac{e_0R^2}{2k_BT\hbar^2}\left(c - \frac{a}{2b}\right)\sqrt{\frac{\pi}{-b}}. \tag{16}$$

Similar to the case of the Holstein model, the parameters of a, b, and c can be calculated using the symmetrized time correlation function defined in Eq. (15) as

$$c = C(\tau_{st}), \tag{17}$$

$$b = \frac{12C''(\tau_{st}) - \sqrt{144C''(\tau_{st})^2 - 48C^{(4)}(\tau_{st})C(\tau_{st})}}{24C(\tau_{st})}, \tag{18}$$

$$a = \frac{C^{(4)}(\tau_{st})}{12b} - \frac{C''(\tau_{st})}{2}, \tag{19}$$

where $C^{(4)}$ denotes the fourth order derivative of $C(t)$. A detailed derivation of the above relations can be found in Appendix B. As in the Holstein model, the real time derivatives can be calculated using the derivatives of $G(\tau)$ defined in Eq. (13) as $C(\tau_{st}) = G(i\tau_{st})$, $C''(\tau_{st}) = -G''(i\tau_{st})$ and $C^{(4)}(\tau_{st}) = G^{(4)}(i\tau_{st})$.

The symmetrized quantum correlation function is an important quantity in quantum dynamics in condensed phase, with applications in problems ranging from reaction rate,[40–42,47,48] quantum dynamical structure factors in liquids,[46,49] and vibrational relaxation rate.[50] In the literature, different ansatzs have been proposed as approximations to the symmetrized real time correlation functions based on its zero time properties.[40–42] We note that the current approximation used in Eq. (15) is justified in the FGR limit, and different forms of ansatzs may be used in future studies.

C. Calculation of the imaginary time current-current correlation function

In Subsection II B, we have obtained the approximate equations for the charge carrier mobility from the imaginary time current-current correlation function. To calculate the imaginary-time correlation function, we perform PIMC calculations based on the method proposed by Cao *et al.*[45] The method was originally developed to simulate the real time quantum dissipative dynamics, and its imaginary time form has recently been used by several group to obtain equilibrium properties of coupled exciton-phonon systems[51] and imaginary time correlation function in charge transfer.[44]

In this method, an imaginary time path property F (to be defined) is calculated as the average over imaginary paths defined using the free phonon bath

$$\langle F[x(\tau)]\rangle_B = \frac{\int dx \int Dx(\tau) F[x(\tau)] e^{-S_\beta^0[x(\tau)]/\hbar}}{\int dx \int Dx(\tau) e^{-S_\beta^0[x(\tau)]/\hbar}}, \quad (20)$$

where $x(0) = x(\hbar\beta) = x$, $S_\beta^0[x(\tau)]$ is the imaginary-time action for the free phonon bath and the functional $F[x(\tau)]$ is to be specified for a given property to calculate.

The above equation provides a convenient way to unravel the effect of the bath degrees of freedom where the bath paths $x(\tau)$ are sampled using the Gaussian integral in the denominator. The following terms $\mathrm{Tr}[j(-i\tau)j(0)e^{-\beta H}]$ and $Z = \mathrm{Tr}e^{-\beta H}$ can then be calculated using Eq. (20) separately, and the imaginary time current-current correlation function $G(\tau)$ can be written as

$$G(\tau) = \frac{1}{Z}\left\langle \mathrm{Tr}\left[e^{-\int_0^{\beta\hbar-\tau} duH(u)/\hbar} j e^{-\int_0^{\tau} duH(u)/\hbar} j\right]\right\rangle_B, \quad (21)$$

where

$$Z = \left\langle \mathrm{Tr} e^{-\int_0^{\hbar\beta} duH(u)/\hbar}\right\rangle_B. \quad (22)$$

The numerical simulation procedure is thus to first sample the bath path $x(\tau)$ according to Eq. (20) and solve the imaginary time Schrödinger equation to get the two terms in Eqs. (21) and (22) to obtain the imaginary time correlation function. Some details of the imaginary time path integral calculation can be found in Ref. 44. The second and fourth order derivatives of $G(\tau)$ are calculated via numerical difference.

III. RESULTS

A. Numerical test of the approximate method for the Holstein model

In this subsection, we first test the accuracy of the saddle point approximation for the Holstein model. From the above Eq. (11), we know that the analytical continuation method actually gives an approximation to the symmetrized correlation function in Eq. (10). By using the numerical exact HEOM method,[52–56] we can calculate the real time current-current correlation function and compare them with the Gaussian approximation in Eq. (11).

In the HEOM calculation for the Holstein model, we use the spectral density defined as follows:

$$J_m(\omega) = \frac{\pi}{2}\sum_{j=1}^{N_b^m} \frac{\left(\alpha_{mj}^{(1)}\right)^2}{\omega_{mj}} \delta(\omega - \omega_{mj}) \quad (23)$$

to describe the local electron-phonon interaction. We also use the Debye spectral density

$$J_m(\omega) = \frac{\eta\gamma\omega}{\omega^2 + \gamma^2}, \quad (24)$$

since it is numerically more efficient for the current HEOM algorithms. The Debye spectral density assumes exponential decay of the bath correlation functions in the high temperature limit and has been used in our previous study of charge carrier mobility.[57]

Similar to our previous work,[58] the conventional current-current correlation function $C(t) = \frac{1}{Z}\mathrm{Tr}[e^{-\beta H}e^{iHt}j(0) \times e^{-iHt}j(0)]$ is calculated by first propagating the coupled electron-phonon system till equilibrium to get the correlated initial state that describes $\rho_{eq} = \frac{1}{Z}e^{-\beta H}$, which is then multiplied with the current operator j as the new initial condition $\tilde{\rho}(0)$ for the real time propagation of the HEOM; the correlation function is then calculated as $\mathrm{Tr}(j\tilde{\rho}(t))$. Details for the HEOM calculation can be referred to our previous works.[57,58] The HEOM simulations are performed with 20 sites in the 1D model. The dynamic filtering parameters are $\delta_1 = 10^{-7}$ for initial equilibration and $\delta_2 = 10^{-10}$ (in atomic units) for correlation function calculations. Converged results are obtained by including the Matsubara frequencies up to $K = 2$, and the largest level of the auxiliary density operators (ADOs) is 10.

After obtaining the correlation function $C(t)$ from the HEOM calculation, we need further to obtain the symmetrized correlation function defined in Eq. (10). We use the following equation connecting the Fourier transforms of the two different kinds of time correlation functions: $\tilde{C}^{sym}(\omega) = e^{-\frac{\beta\omega}{2}}\tilde{C}(\omega)$, where the Fourier transform of the correlation function $C(t)$ is defined as $\tilde{C}(\omega) = \int_{-\infty}^{+\infty} e^{-i\omega t}C(t)dt$. Thus, we first calculate $\tilde{C}(\omega)$ from $C(t)$, then obtain $\tilde{C}(\omega)$, and finally $C^{sym}(t)$ via $C^{sym}(t) = \frac{1}{2\pi}\int_{-\infty}^{+\infty} d\omega e^{i\omega t}e^{-\frac{\beta\omega}{2}}\tilde{C}(\omega)$.

Results of simulations with the following set of parameters $T = 300$ K, $\eta = 323$ cm^{-1}, and $\gamma = 41$ cm^{-1} for two different intermolecular couplings $J = 50$ cm^{-1} and $J = 400$ cm^{-1} are

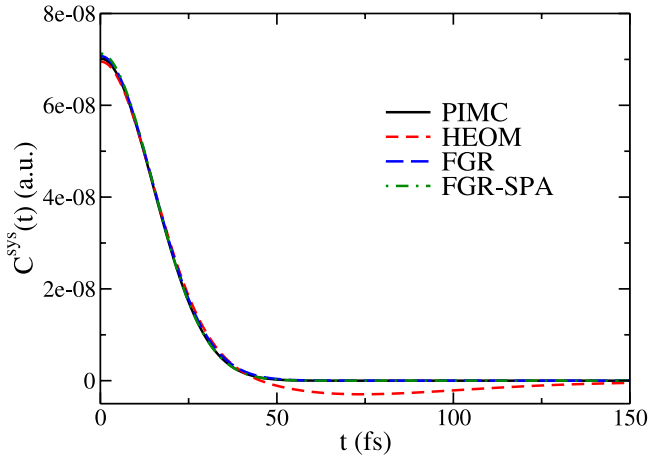

FIG. 1. Symmetrized current-current correlation function calculated for the Holstein model with a Debye spectral density described in Sec. III A, using different methods: PIMC and analytical continuation (solid, black), numerically exact HEOM (dashed, red), FGR (long dashed, blue), and FGR-SPA (dashed-dotted, green). The intermolecular electronic coupling is $J = 50\ \mathrm{cm}^{-1}$.

shown in Figs. 1 and 2. We can see that the symmetrized correlation function calculated by the analytical continuation agrees very well with the HEOM result, especially at short times. We note that with the Gaussian ansatz, the approximate correlation function is always positive, so it misses the negative features of the numerical exact result at longer time. However, since the symmetrized correlation function decays quickly and we are more interested in the integral of the real time correlation function, this should only lead to small errors to the charge carrier mobility.

We have also compared with the correlation functions from the second order perturbation approximation via the FGR derived in Appendix A, where it is also shown to be the same as the result by Hannewald and Bobbert in the special case of the Holstein model.[21,24] Results from the SPA to the FGR (FGR-SPA) are also presented. It is found that the correlation function based on the FGR approximation agrees well with the exact result in small coupling case $J = 50\ \mathrm{cm}^{-1}$ (Fig. 1) but significantly overestimate the current-current correlation function in the strong coupling case $J = 400\ \mathrm{cm}^{-1}$ (Fig. 2).

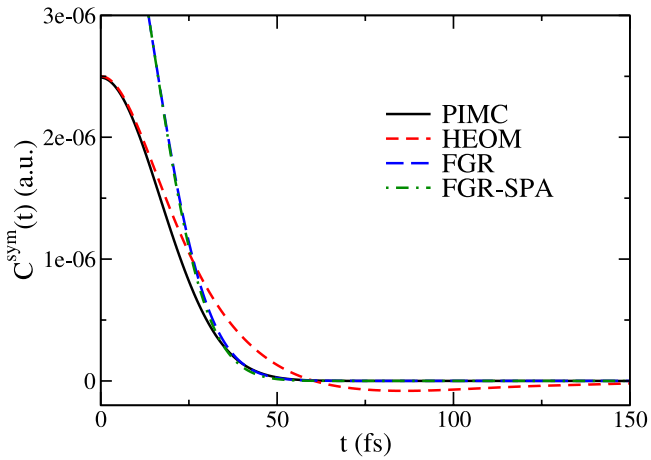

FIG. 2. Same as Fig. 1, for $J = 400\ \mathrm{cm}^{-1}$.

In this work, benchmark tests using the HEOM method are only performed in the case of local electron-phonon coupling (the Holstein model). Applications of the HEOM method to study the Holstein-Peierls model are certainly possible, by including fluctuations of transfer integral as in our previous work.[57] However, the current-current correlation function $C(t)$ in the Holstein-Peierls model includes bath operators that cannot be described by the reduce density operator of the system degrees of freedom. This will require a new set of equations to calculate correlation functions involving bath coordinates from the HEOM formalism and is beyond the scope of this work, which is mainly on the imaginary time path integral method. We also note that the benchmark HEOM calculations are only performed with a dissipative bath, and not with single-mode electron-phonon coupling models (see the next subsection below). Although the HEOM method is able to treat undamped harmonic oscillator modes,[59] the current approach to obtain the thermal equilibrium state is not applicable for single mode models, due to the lack of dissipation in the electron-phonon coupling terms. New methods are to be developed to treat this problem and are subjected to future publications.

B. Parameters for the Holstein and Holstein-Peierls models

In Subsections III C and III D, calculations of the charge carrier mobility are performed with the approximate methods presented in Sec. II B. We adopt the following model parameters that have been used in previous calculations using the diffusion constant method,[27,29,60] where the many vibrational modes are represented by one effective mode on each site for a given type of electron-phonon coupling. The distance between neighbouring sites in the 1D tight-binding model is set to be $R = 5$ Å. In the Holstein model, we use one effective vibrational mode for each site, with the vibrational frequency $\omega_1 = 40\ \mathrm{cm}^{-1}$, the effective mass $m_1 = 250$ amu, and the local electron-phonon coupling constant $\alpha_1 \equiv \alpha^{(1)} = 3500\ \mathrm{cm}^{-1}/\text{Å}$. Four different values of the transfer integral $J = 50$, 100, 200, and 400 cm^{-1} are used in the simulations. Numerical tests show that a 1D model with up to 20 sites is enough to give converged imaginary time correlation functions regarding the system size.

For the Holstein-Peierls model, we keep all the above parameters for the local electron-phonon coupling and introduce a second effective harmonic oscillator mode to describe the nonlocal electron-phonon coupling. The vibrational frequency of the new vibrational mode, ω_2, is also set to 40 cm^{-1}, $m_2 = 250$ amu, and two different values for the non-local electron-phonon coupling constant $\alpha_2 \equiv \alpha^{(2)} = 500\ \mathrm{cm}^{-1}/\text{Å}$ and $1000\ \mathrm{cm}^{-1}/\text{Å}$ are used in the simulations.

C. The Holstein model

In this and Subsection III D, we will also present some equilibrium properties to help understand the mechanism of charge carrier transport. Such properties characterize the "size" of the polaron and the delocalization of the charge carrier and are readily obtained using imaginary time path

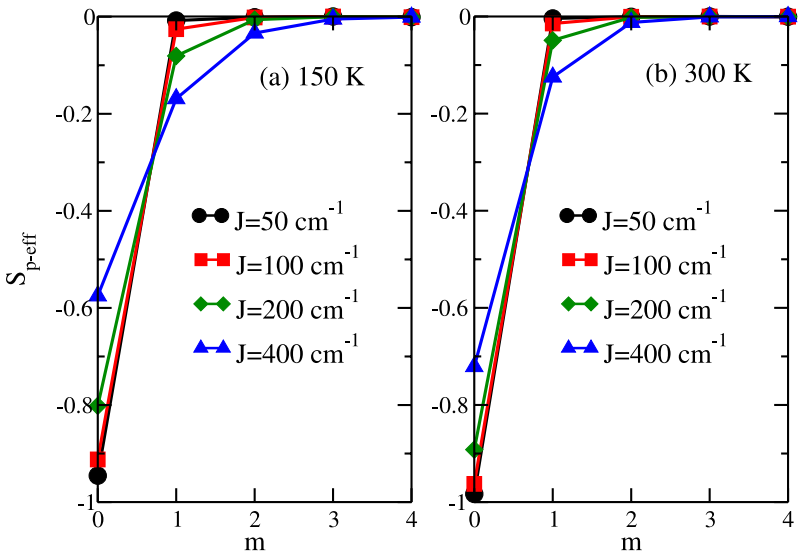

FIG. 3. Equilibrium polaron deformation effect calculated using Eq. (25) for the Holstein model described in Sec. III C, with different intermolecular coupling strengths: (a) $T = 150$ K and (b) $T = 300$ K.

integral calculations. The first such quantity is the strength of polaron deformation which is defined as the average of the electron-phonon coupling times the population operator, scaled by the reorganization energy

$$S_m = \frac{1}{2\lambda} \sum_n \left\langle \alpha_1 x_{m+n} a_n^+ a_n \right\rangle, \tag{25}$$

where $\lambda = \frac{\alpha_1^2}{2m\omega_1^2}$. In the case $J = 0$ for isolated molecules, we have $S_0 = -1$ and $S_m = 0$, $m \neq 0$. This property has also been used by Lindenberg and coworkers[61] and other groups[62,63] to study the polaron self-trapping transition.

The equilibrium density matrix contains information on the charge carrier delocalization. In a previous paper, we have used the amplitude of the off-diagonal terms of the reduced density matrix to characterize the delocalization of the polaron.[57] In this work, we use the coherence length L_ρ defined as[64]

$$L_\rho = \left[\left(\sum_{ij} |\rho_{ij}| \right)^2 \right] \left[M \sum_{ij} |\rho_{ij}|^2 \right]^{-1}. \tag{26}$$

Fig. 3 shows the polaron deformation defined in Eq. (25) for the Holstein model with different intermolecular coupling strengths. We can see that for $J = 400$ cm^{-1}, the polaron deformation distributes over several sites due to charge delocalization. As the coupling strength J decreases, the charge becomes more localized, and the polaron deformation effect is essentially localized on one site. It can be seen that the polaron size decreases when the temperature increases.

The coherence length L_ρ defined in Eq. (26) is calculated with different intermolecular coupling strengths at various temperatures, and the result is shown in Fig. 4. It can be seen that L_ρ increases with larger J value and lower temperature, which show similar trends as in Fig. 3 for the polaron deformation effect S.

The imaginary time current-current correlation function is then calculated and Eq. (14) is used to calculate the charge carrier mobility. Fig. 5 shows the imaginary time correlation functions with two different electronic couplings $J = 50$ cm^{-1} and $J = 400$ cm^{-1}. Fig. 6 shows the temperature dependence of charge carrier mobility with different electron coupling strengths. It can be seen that for small electronic coupling $J = 50$ cm^{-1}, the charge carrier transport is dominated by thermally activated process where the mobility first increases at low temperature. By investigating the polaron polarization effects and the coherence length in Figs. 3 and 4, we know that the polaron is essentially localized on one site, and the charge transport mechanism is hopping between neighbouring sites. When $J = 400$ cm^{-1}, it can be seen that the charge carrier is delocalized over several sites (about 5 at 300 K, as seen in Fig. 4), and the mobility exhibits a typical power law $\mu(T) \sim 1/T^\alpha$, which indicates that the transport is in the band-like regime.

From the above simulations of the Holstein model with different parameters, we can see that the analytical continuation method captures the crossover form band-like to hopping transport when reducing the intermolecular coupling strength.[29,65] The calculated charge carrier mobilities also agree with the recent studies using the surface hopping simulations,[30] which does not have the drawbacks of the mean field approach in the hopping regime. Another advantage of the imaginary time path integral calculation is that it provides

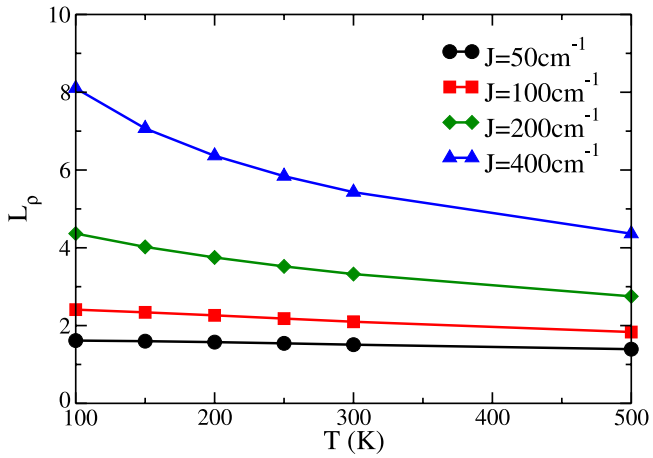

FIG. 4. Temperature dependence of the equilibrium coherence length in the Holstein model described in Sec. III C, with different intermolecular electronic couplings.

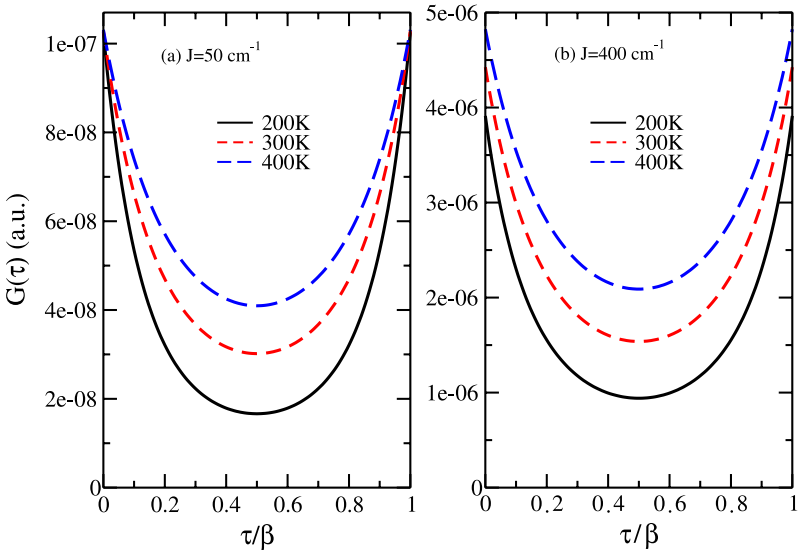

FIG. 5. Imaginary-time current-current correlation function calculated from the imaginary time PIMC approach at different temperatures: (a) $J = 50\ \mathrm{cm}^{-1}$ and (b) $J = 400\ \mathrm{cm}^{-1}$.

exact equilibrium properties such as the polaron effect and the charge delocalization effect, which helps in analyzing the transport mechanisms.

D. The Holstein-Peirels model

In this subsection, we investigate the additional effect of nonlocal electron-phonon coupling by comparing the results with those of the Holstein model where only the effect of local electron-phonon coupling is considered.

The coherence lengths are first calculated with two different intermolecular coupling strengths, as well as different strengths of nonlocal electron-phonon coupling, which are compared with those from the Holstein model ($\alpha_2 = 0$). Fig. 7(a) shows the result with electron coupling $J = 50\ \mathrm{cm}^{-1}$. We can see that the coherence length is larger with $\alpha_2 = 500\ \mathrm{cm}^{-1}/\text{Å}$ than that in the Holstein model ($\alpha_2 = 0$) and is even larger with $\alpha_2 = 1000\ \mathrm{cm}^{-1}/\text{Å}$, which indicates that fluctuation on electron coupling tends to delocalize the charge

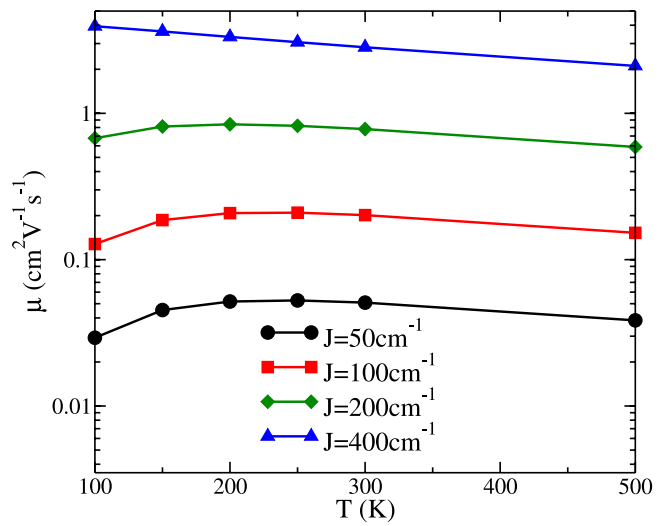

FIG. 6. Temperature dependence of charge carrier mobility for the Holstein model described in Sec. III C with different electronic coupling strengths.

in the hopping regime. In Fig. 7(b) with $J = 400\ \mathrm{cm}^{-1}$, the coherence length with $\alpha_2 = 500\ \mathrm{cm}^{-1}/\text{Å}$ is smaller than that in the Holstein model ($\alpha_2 = 0$), and the larger $\alpha_2 = 1000\ \mathrm{cm}^{-1}/\text{Å}$ leads to even smaller coherence length. Within this set of parameters, the coherence length L_ρ is not very sensitive to the nonlocal electron-phonon coupling constant α_2. However, an inverse trend for the change of L_ρ with different α_2's is clearly observed in Fig. 7 for $J = 50\ \mathrm{cm}^{-1}$ and $J = 400\ \mathrm{cm}^{-1}$. This indicates that the nonlocal electron-phonon coupling destroys the coherence between different sites and leads more localized charges in the band-like regime.

It is thus expected that the non-local electron-phonon coupling may have different effects on the charge carrier mobility in the hopping and band-like regimes. The calculated charge carrier mobilities are shown in Fig. 8 for the intermolecular coupling strength $J = 50\ \mathrm{cm}^{-1}$ and $J = 400\ \mathrm{cm}^{-1}$, respectively. In the hopping regime, increasing the strength of the non-local electron-phonon coupling leads to increased mobility, while in the band-like regime, the charge carrier mobility decreases with the increase of the non-local electron-phonon coupling. This trend agrees with the previous finding when only the non-local electron-phonon coupling is considered.[57] Such behavior of polaron transport is also consistent with the calculation of the coherence length presented in Fig. 7.

From the above calculations, we can see that the local and nonlocal electron-phonon couplings have different effects on charge carrier delocalization and transport. Increasing local electron-phonon coupling will always increase the polaron effect and localization of the charge carrier regardless of the intermolecular electronic coupling strength. However, the situation is different for the non-local electron-phonon coupling. With small intermolecular electronic coupling, where charge transport is in the hopping regime, increasing nonlocal electron-phonon coupling will actually increase the effective intermolecular coupling and may lead to larger charge carrier delocalization and larger charge carrier mobility. When the intermolecular electronic coupling is large, the charge transport is band-like and the polaron is delocalized over several sites. In such a case, increasing local and nonlocal electron-

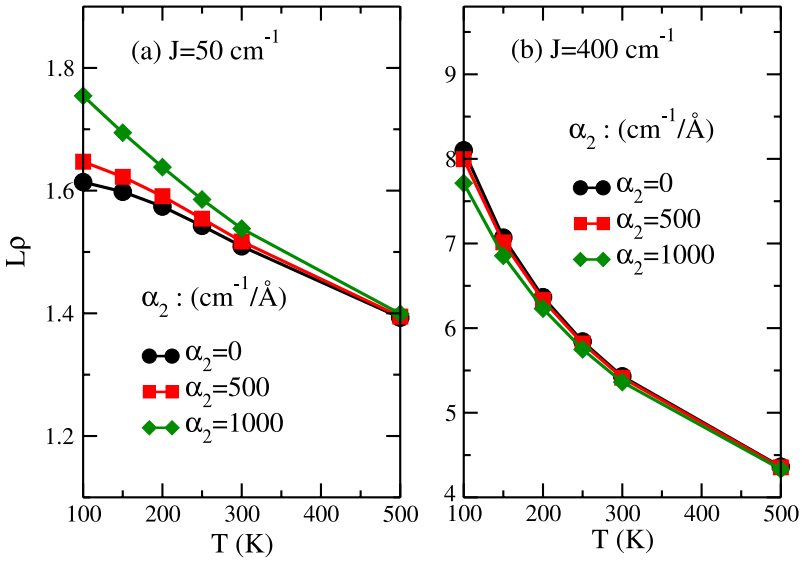

FIG. 7. Equilibrium coherence length of the Holstein-Peierls model described in Sec. III D, with different α_2 coefficients for the nonlocal electron-phonon coupling. (a) $J = 50\ \mathrm{cm}^{-1}$ and (b) $J = 400\ \mathrm{cm}^{-1}$.

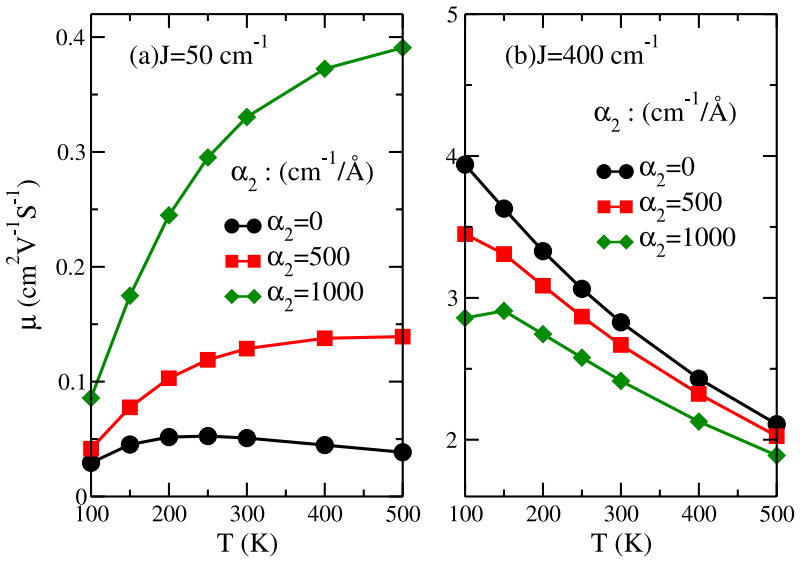

FIG. 8. Charge carrier mobility for the Hosltein-Peierls model as a function of temperature with different nonlocal electron-phonon coupling constants $\alpha_2 = 0$ (the Holstein model), 500 $\mathrm{cm}^{-1}/\text{Å}$, and 1000 $\mathrm{cm}^{-1}/\text{Å}$. (a) $J = 50\ \mathrm{cm}^{-1}$ and (b) $J = 400\ \mathrm{cm}^{-1}$.

phonon couplings both destroy the intermolecular coherence, which leads to more localized polaron and reduced mobility.

IV. CONCLUSIONS AND DISCUSSIONS

In this paper, an approximate method using imaginary time path integral Monte Carlo simulation is proposed to study the charge carrier transport properties in OMCs. The new method is based on the saddle point approximation to perform analytical continuation calculation of the Kubo formula for charge carrier mobility.

A major advantage of the new method is that it is not limited to perturbative calculations as in many of the analytical theories. At the same time, it also gives the correct equilibrium properties. As is found out, for the Holstein model with only local electron-phonon coupling, the SPA is equivalent to the Gaussian approximation for the symmetrized current-current correlation function. For the Holstein-Peierls model that considers both the local and nonlocal electron-phonon couplings, a new analytical ansatz is proposed for the analytical continuation.

To test the validity of the SPA, we employ the numerically exact non-perturbation HEOM method to perform benchmark calculations with the Debye spectral density in the Holstein model. It is shown that the Gaussian type assumption for the symmetrized time correlation function agrees reasonably well with the numerically exact results.

We then apply the approximate method to study the charge mobility behavior in OMCs for the Holstein and Holstein-Peierls models. To better understand the underlying charge transfer mechanism, we have also calculated the equilibrium properties including the polaron deformation effect and the coherence length to characterize the polaron deformation and charge delocalization effects. Our calculation of the temperature dependence of the mobility shows crossover from the band-like to the hopping in mobility in certain parameter ranges. The different effects caused by local and nonlocal electron-phonon couplings are then studied. It is shown that increasing the local electron-phonon coupling always localizes the charge carrier and reduces the mobility. In the band-like transport regime, the nonlocal electron phonon coupling described by the Peierls term has the same effect as the local electron-phonon coupling, while in the hopping regime, larger

nonlocal electron-phonon coupling tends to delocalize the charge carrier and increase the mobility.

ACKNOWLEDGMENTS

This work is supported by NSFC (Grant No. 21290194), the 973 program (Grant Nos. 2011CB808502 and 2013CB933501), and the Strategic Priority Research Program of the Chinese Academy of Sciences (Grant No. XDB12020300).

APPENDIX A: CURRENT-CURRENT CORRELATION FUNCTION FROM SECOND ORDER PERTURBATION

In this Appendix, we calculate the current-current correlation function based on second order perturbation (also termed as the FGR approximation in Sec. III A). For simplicity, we consider only two modes for each site that describes the local and nonlocal electron phonon couplings, where

$$H_{e-ph} = \sum_{m=1}^{N} \alpha_1 x_{m1} |m\rangle\langle m| + \sum_{m=1}^{N} \alpha_2 x_{m2} (|m\rangle\langle m+1| + |m+1\rangle\langle m|), \quad \text{(A1)}$$

while generalization of the result to multi-mode case is straightforward.

With Eq. (A1), the current operator in the Holstein-Peierls model is written as

$$j = -i \sum_{m=1}^{N} (-J + \alpha_2 x_{m2})(|m\rangle\langle m+1| - |m+1\rangle\langle m|). \quad \text{(A2)}$$

So the current-current correlation can be calculated as

$$\begin{aligned} C(t) &= \langle e^{iHt/\hbar} j(0) e^{-iHt\hbar} j(0)\rangle \\ &= \frac{1}{Z} \int_{-\infty}^{\infty} d\mathbf{Q} \sum_{m=1}^{N} \langle \mathbf{Q}|\langle m| e^{-\beta H} e^{iHt/\hbar} \\ &\quad \times j(0)\, e^{-iHt\hbar} j(0)|m\rangle|\mathbf{Q}\rangle, \end{aligned} \quad \text{(A3)}$$

where Z is partition function and $|\mathbf{Q}\rangle = |x_{11}, x_{12}, \ldots, x_{N1}, x_{N2}\rangle$ represents the nuclear degrees of freedom.

The second order perturbation is done by neglecting all the off-diagonal terms of H in the real and imaginary time propagators within the above equation when calculating the correlation function. After some simplification, we obtain the following equation:

$$\begin{aligned} C(t) \approx -\sum_m \frac{1}{Z} \int_{-\infty}^{\infty} d\mathbf{Q}_m \langle \mathbf{Q}_m| e^{-\beta h_m} e^{ih_m t/\hbar} (-J + \alpha_2 x_{m2}) \\ \times e^{-i\tilde{h}_{m+1} t/\hbar} (-J + \alpha_2 x_{m2}) + e^{-\beta \tilde{h}_{m+1}} e^{i\tilde{h}_{m+1} t/\hbar} \\ \times (J - \alpha_2 x_{m2}) e^{-ih_m t/\hbar} (J - \alpha_2 x_{m2}) |\mathbf{Q}_m\rangle, \end{aligned} \quad \text{(A4)}$$

where $|\mathbf{Q_m}\rangle = |x_{m1}, x_{m2}, x_{m+1,1}\rangle$, and

$$\begin{aligned} h_m = \frac{p_{m1}^2}{2M_{m1}} + \frac{1}{2} M_{m1} \omega_{m1}^2 x_{m1}^2 + \alpha_1 x_{m1} + \frac{p_{m+1,1}^2}{2M_{m+1,1}} \\ + \frac{1}{2} M_{m+1,1} \omega_{m+1,1}^2 x_{m+1,1}^2 + \frac{p_{m2}^2}{2M_{m2}} + \frac{1}{2} M_{m2} \omega_{m2}^2 x_{m2}^2, \end{aligned} \quad \text{(A5)}$$

$$\begin{aligned} \tilde{h}_{m+1} = \frac{p_{m+1,1}^2}{2M_{m+1,1}} + \frac{1}{2} M_{m+1,1} \omega_{m+1,1}^2 x_{m+1,1}^2 + \alpha_1 x_{m+1,1} \\ + \frac{p_{m,1}^2}{2M_{m,1}} + \frac{1}{2} M_{m1} \omega_{m1}^2 x_{m1}^2 + \frac{p_{m2}^2}{2M_{m2}} + \frac{1}{2} M_{m2} \omega_{m2}^2 x_{m2}^2. \end{aligned} \quad \text{(A6)}$$

Further calculations lead to the following equation for the current-current correlation function:

$$C(t) = \left(2J^2 + \frac{\alpha_2^2 \hbar \Phi_2}{m\omega_2}\right) \exp\left\{-\frac{\alpha_1^2}{\hbar m \omega_1^3} [1 + 2N_1 - \Phi_1]\right\}, \quad \text{(A7)}$$

where $\Phi_k = (1 + N_k) e^{-i\omega_k t} + N_k e^{i\omega_k t}$; $N_k = 1/(e^{\hbar\omega_k / k_B T} - 1)$; $k = 1, 2$. The charge carrier mobility is then given by

$$\begin{aligned} \mu(T) = \frac{e_0 R^2}{2k_B T \hbar^2} \sum_m \int_{-\infty}^{+\infty} dt \left(2J^2 + \frac{\alpha_2^2 \hbar \Phi_2}{m\omega_2}\right) \\ \times \exp\left\{-\frac{\alpha_1^2}{\hbar m \omega_1^3} [1 + 2N_1 - \Phi_1]\right\}. \end{aligned} \quad \text{(A8)}$$

For the special case of the Holstein model, the nonlocal electron-phonon coupling constants α_2 are set to 0, so the above equations become

$$C(t) = 2J^2 \exp\{-\frac{\alpha_1^2}{\hbar m \omega_1^3} [1 + 2N_1 - \Phi_1]\} \quad \text{(A9)}$$

and

$$\mu(T) = \frac{e_0 R^2}{2k_B T \hbar^2} \sum_m \int_{-\infty}^{+\infty} dt 2J^2 e^{-\frac{\alpha_1^2}{\hbar m \omega_1^3} [1 + 2N_1 - \Phi_1(t)]}. \quad \text{(A10)}$$

It can be shown that, in the special case of the Holstein model, the above result in Eq. (A10) for the charge carrier mobility is the same as that obtained by Hannewald and Bobbert.[21]

In the remaining parts of this Appendix, we justify the usage of the ansatz in Eq. (15) for the Holstein-Peierls model. By defining $A = 2J^2$, $B = \frac{\alpha_2^2 \hbar}{m\omega_2}$, and $C = -\frac{\alpha_1^2}{\hbar m \omega_1^3}$, the correlation $C(t)$ in Eq. (A7) becomes

$$C(t) = [A + B\Phi_2(t)] e^{C[1 + 2N_1 - \Phi_1(t)]}; \quad \text{(A11)}$$

after shifting it to the saddle point $\tau_{st} = -\frac{i\hbar\beta}{2}$, we get

$$C(\tau_{st} + t) = [A + B\Phi_2(\tau_{st} + t)] e^{C[1 + 2N_1 - \Phi_1(\tau_{st} + t)]}, \quad \text{(A12)}$$

where

$$\Phi_k(\tau_{st} + t) = (1 + N_k) e^{-\beta\hbar\omega_k/2} e^{-i\omega_k t} + N_k e^{\beta\hbar\omega_k/2} e^{i\omega_k t}, \quad \text{(A13)}$$

for $k = 1, 2$. After making the short time expansion $e^{i\omega t} \approx 1 + i\omega t - \frac{(\omega t)^2}{2}$,

$$\begin{aligned} C(\tau_{st} + t) \approx \left\{A + B\left[(1 + N_2) e^{-\beta\hbar\omega_2/2} + N_2 e^{\beta\hbar\omega_2/2}\right]\right. \\ \times \left.\left(1 - \frac{(\omega_2 t)^2}{2}\right)\right\} \exp\left\{C\left[1 + 2N_1\right.\right. \\ \left.\left. - [(1 + N_1) e^{-\beta\hbar\omega_1/2} + N_1 e^{\beta\hbar\omega_1/2}]\left(1 - \frac{(\omega_1 t)^2}{2}\right)\right]\right\}. \end{aligned} \quad \text{(A14)}$$

The above equation thus justifies the ansatz in Eq. (15) in the perturbation limit.

APPENDIX B: SADDLE POINT APPROXIMATION OF EQ. (A10)

For the Holstein model, the saddle point approximation of Eq. (A10) can be obtained as a special case of Eq. (A14), which is given by

$$C(\tau_{st}+t) \approx 2J^2 \exp\Big\{-\frac{\alpha_1^2}{\hbar m\omega_1^3}\Big[1+2N_1-[(1+N_1)\times e^{-\beta\hbar\omega_1/2}+N_1 e^{\beta\hbar\omega_1/2}]\Big(1-\frac{(\omega_1 t)^2}{2}\Big)\Big]\Big\}. \quad \text{(B1)}$$

APPENDIX C: DERIVATION OF EQS. (17)–(19)

In this appendix, we calculate the parameters a, b, and c from the symmetrized real time correlation function $C(\tau_{st}+t)$ through the ansatz $C(\tau_{st}+t) = (c+at^2)e^{bt^2}$, which gives

$$C''(\tau_{st}+t) = 2ae^{bt^2} + 4abt^2e^{-bt^2} + 2b(c+3at^2)e^{bt^2} + 4b^2(ct^2+at^4)e^{bt^2}, \quad \text{(C1)}$$

$$C^{(4)}(\tau_{st}+t) = (24ab+12b^2c)e^{bt^2} + 2b(24ab+12b^2c)t^2e^{bt^2} + 3(36ab^2+8b^3c)t^2e^{bt^2} + 2b(36ab^2+8b^3c)t^4e^{bt^2} + 40ab^3t^4e^{bt^2} + 16ab^4t^6e^{bt^2}. \quad \text{(C2)}$$

At the saddle point ($t = 0$), we have

$$C(\tau_{st}) = c, \quad \text{(C3)}$$

$$C''(\tau_{st}) = 2(a+bc), \quad \text{(C4)}$$

$$C^{(4)}(\tau_{st}) = 12b(2a+bc). \quad \text{(C5)}$$

By solving the above equations, we get

$$c = C(\tau_{st}), \quad \text{(C6)}$$

$$b = \frac{12C''(\tau_{st}) - \sqrt{144C''^2(\tau_{st}) - 48C^{(4)}(\tau_{st})C(\tau_{st})}}{24C(\tau_{st})}, \quad \text{(C7)}$$

$$a = \frac{C^{(4)}(\tau_{st})}{12b} - \frac{C''(\tau_{st})}{2}, \quad \text{(C8)}$$

which are just Eqs. (17)–(19).

[1]S. R. Forrest, Org. Electron. **4**, 45 (2003).
[2]H. Sirringhaus, N. Tessler, and R. H. Friend, Science **280**, 1741 (1998).
[3]M. E. Gershenson, V. Podzorov, and A. F. Morpurgo, Rev. Mod. Phys. **78**, 973 (2006).
[4]H. Klauk, U. Zschieschang, J. Pflaum, and M. Halik, Nature **445**, 745 (2007).
[5]M. Granstrom, K. Petritsch, A. C. Arias, A. Lux, M. R. Andersson, and R. H. Friend, Nature **395**, 257 (1998).
[6]H. Spanggaard and F. C. Krebs, Sol. Energy Mater. Sol. Cells **83**, 125 (2004).
[7]V. Coropceanu, J. Cornil, D. A. da Silva Filho, Y. Oliver, R. Silbey, and J. L. Brédas, Chem. Rev. **107**, 926 (2007).
[8]N. Karl, Synth. Met. **133**, 649 (2003).
[9]T. Holstein, Ann. Phys. **8**, 325 (1959).
[10]E. A. Silinsh and V. Capek, *Organic Molecular Crystals: Interaction, Localization, and Transport Phenomena* (AIP Press, New York, 1994).
[11]R. Silbey and R. W. Munn, J. Chem. Phys. **72**, 2763 (1980).
[12]V. M. Kenkre, J. D. Andersen, D. H. Dunlap, and C. B. Duke, Phys. Rev. Lett. **62**, 1165 (1989).
[13]S. Fratini and S. Ciuchi, Phys. Rev. Lett. **91**, 256403 (2003).
[14]T. Holstein, Ann. Phys. **8**, 343 (1959).
[15]P. Gosar and S. Choi, Phys. Rev. **150**, 529 (1966).
[16]A. Troisi, Chem. Soc. Rev. **40**, 2347 (2011).
[17]M. E. Pope and C. E. Swenberg, *Electronic Processes in Organic Crystals and Polymers*, 2nd ed. (Oxford University Press, New York, 1999).
[18]N. Karl, in *Organic Electronic Materials: Conjugated Polymers And Low Molecular Weight Organic Solids*, Springer Series in Materials Science, Vol. 41, edited by R. Farchioni and G. Grosso (Springer-Verlag, Berlin, 2001), pp. 283–326.
[19]Y.-C. Cheng, R. J. Silbey, D. A. da Silva Filho, J. P. Calbert, J. Cornil, and J. Bredas, J. Chem. Phys. **118**, 3764 (2003).
[20]G. J. Nan, X. D. Yang, L. J. Wang, Z. Shuai, and Y. Zhao, Phys. Rev. B **79**, 115203 (2009).
[21]K. Hannewald and P. A. Bobbert, Appl. Phys. Lett. **85**, 1535 (2004).
[22]R. W. Munn and R. Silbey, J. Chem. Phys. **83**, 1843 (1985).
[23]R. W. Munn and R. Silbey, J. Chem. Phys. **83**, 1854 (1985).
[24]K. Hannewald and P. A. Bobbert, Phys. Rev. B **69**, 075212 (2004).
[25]K. Hannewald, V. M. Stojanovic, J. M. T. Schellekens, P. A. Bobbert, G. Kresse, and J. Hafner, Phys. Rev. B **69**, 075211 (2004).
[26]F. Ortmann, F. Bechstedt, and K. Hannewald, Phys. Status Solidi B **248**, 511 (2011).
[27]A. Troisi and G. Orlandi, Phys. Rev. Lett. **96**, 086601 (2006).
[28]M. Hultell and S. Stafström, Chem. Phys. Lett. **428**, 446 (2006).
[29]L. Wang and D. Beljonne, J. Phys. Chem. Lett. **4**, 1888 (2013).
[30]L. Wang and D. Beljonne, J. Chem. Phys. **139**, 064316 (2013).
[31]G. Mahan, *Many-Particle Physics* (Plenum Press, London, 1990).
[32]*Classical and Quantum Dynamics in Condensed Phase Simulations*, edited by B. J. Berne, G. Ciccotti, and D. F. Coker (World Scientific, New Jersey, 1998).
[33]D. M. Ceperley, Rev. Mod. Phys. **67**, 279 (1995).
[34]M. Jarrell and J. E. Gubernatis, Phys. Rep. **269**, 133 (1996).
[35]S. A. Egorov and J. L. Skinner, J. Chem. Phys. **105**, 7047 (1996).
[36]D. Kim, J. D. Doll, and J. E. Gubernatis, J. Chem. Phys. **106**, 1641 (1997).
[37]E. Rabani, G. Krilov, and B. J. Berne, J. Chem. Phys. **112**, 2605 (2000).
[38]W. H. Miller, J. Chem. Phys. **62**, 1899 (1975).
[39]P. G. Wolynes, J. Chem. Phys. **87**, 6559 (1987).
[40]N. F. Hansen and H. C. Andersen, J. Phys. Chem. **100**, 1137 (1996).
[41]M. Ceotto, S. Yang, and W. H. Miller, J. Chem. Phys. **122**, 044109 (2005).
[42]J. Vaníček, W. H. Miller, J. F. Castillo, and F. J. Aoiz, J. Chem. Phys. **123**, 054108 (2005).
[43]S. Yang and J. S. Cao, J. Chem. Phys. **122**, 094108 (2005).
[44]G.-J. Nan, Q. Shi, Z.-G. Shuai, and Z.-S. Li, Phys. Chem. Chem. Phys. **13**, 9736 (2011).
[45]J. Cao, L. W. Ungar, and G. A. Voth, J. Chem. Phys. **104**, 4189 (1996).
[46]P. Schofield, Phys. Rev. Lett. **4**, 239 (1960).
[47]W. H. Miller, S. D. Schwartz, and J. W. Tromp, J. Chem. Phys. **79**, 4889 (1983).
[48]W. H. Miller, M. C. Y. Zhao, and S. Yang, J. Chem. Phys. **119**, 1329 (2003).
[49]M. Monteferrante, S. Bonella, and G. Ciccotti, J. Chem. Phys. **138**, 054118 (2013).
[50]F. X. Vázquez, I. Navrotskaya, and E. Geva, J. Phys. Chem. A **114**, 5682 (2010).
[51]J. M. Moix, Y. Zhao, and J. Cao, Phys. Rev. B **85**, 115412 (2012).
[52]Y. Tanimura, J. Phys. Soc. Jpn. **75**, 082001 (2006).
[53]Y. Yan, F. Yang, Y. Liu, and J. Shao, Chem. Phys. Lett. **395**, 216 (2004).
[54]R.-X. Xu, P. Cui, X.-Q. Li, Y. Mo, and Y.-J. Yan, J. Chem. Phys. **122**, 041103 (2005).
[55]A. Ishizaki and Y. Tanimura, J. Phys. Soc. Jpn. **74**, 3131 (2005).
[56]Q. Shi, L. P. Chen, G. J. Nan, R. X. Xu, and Y. J. Yan, J. Chem. Phys. **130**, 084105 (2009).
[57]D. Wang, L. P. Chen, R. H. Zheng, L. J. Wang, and Q. Shi, J. Chem. Phys. **132**, 081101 (2010).
[58]Y.-Y. Jing, L.-P. Chen, S.-M. Bai, and Q. Shi, J. Chem. Phys. **138**, 045101 (2013).
[59]H. Liu, L. Zhu, S. Bai, and Q. Shi, J. Chem. Phys. **140**, 134106 (2014).
[60]L. Wang, D. Beljonne, L. Chen, and Q. Shi, J. Chem. Phys. **134**, 244116 (2011).
[61]A. H. Romero, D. W. Brown, and K. Lindenberg, Phys. Rev. B **59**, 13728 (1999).
[62]M. Zoli, Adv. Condens. Matter Phys. **2010**, 815917.
[63]L.-C. Ku, S. A. Trugman, and J. Bonča, Phys. Rev. B **65**, 174306 (2002).
[64]A. Damjanović, I. Kosztin, U. Kleinekathöfer, and K. Schulten, Phys. Rev. E **65**, 031919 (2002).
[65]Y.-C. Cheng and R. J. Silbey, J. Chem. Phys. **128**, 114713 (2008).